Journal of Materials Chemistry B

ROYAL SOCIETY OF CHEMISTRY

PAPER



Cite this: J. Mater. Chem. B, 2023, 11, 2490

# Interaction of polyelectrolyte-shell cubosomes with serum albumin for triggering drug release in gastrointestinal cancer

Barbara V. Pimenta,[a] Rafael R.M. Madrid,[a] Patrick D. Mathews,[a] Karin A. Riske,[a] Watson Loh,[b] Borislav Angelov,[c] Angelina Angelova*[d] and Omar Mertins *[ad]

Received 8th December 2022,
Accepted 3rd February 2023

DOI: 10.1039/d2tb02670h

rsc.li/materials-b

Nano-structured and functionalized materials for encapsulation, transport, targeting and controlled release of drugs are of high interest to overcome low bioavailability in oral administration. We develop lipid-based cubosomes, which are surface-functionalized with biocompatible chitosan-*N*-arginine and alginate, displaying internal liquid crystalline structures. Polyelectrolyte-shell (PS) cubosomes have pH-responsive characteristics profitable for oral delivery. The obtained PScubosomes can strongly interact with serum albumin, a protein which is released in the stomach under gastric cancer conditions. An effective thermodynamic PScubosome–protein interaction was characterized at pH 2.0 and 7.4 by isothermal titration calorimetry at 37 °C. A high increment of the albumin conformation transition temperature was evidenced by differential scanning calorimetry upon incubation with PScubosomes. The performed structural studies by synchrotron small-angle X-ray scattering (SAXS) revealed essential alterations in the internal liquid crystalline topology of the nanocarriers including an *Im3m* to *Pn3m* transition and a reduction of the cubic lattice parameters. The PScubosome nanoparticle interaction with serum albumin, leading to inner structural changes in a range of temperatures, promoted the release of water from the cubosomal nanochannels. Altogether, the results revealed effective interactions of the PScubosomes with albumin under simulated gastrointestinal pH conditions and suggested promising nanocarrier characteristics for triggered oral drug release.

## Introduction

Gastrointestinal cancers include a large range of clinical conditions and diseases, which require different treatment approaches with regular or high specificity.[1,2] Despite the gradual improvement of anticancer treatments, problems related to severe side effects of the available chemotherapies still persist.[3–5] Advances in nanotechnology constantly provide new tools and strategies for human medical diagnostics and therapeutic treatments.[6,7] In this regard, the development of nanoparticles, specifically designed as drug delivery systems, increases the opportunities for safe and more efficiently targeted cancer therapies.[8–13] The enhanced performance of the drug delivery devices depends on specificities related to compositional features that ensure their effective interactions with the biological milieu, organs, and tissues.[14]

Concerning the gastrointestinal tract condition, it has been reported that massive leakage of serum albumin into the gastric lumen is produced in gastric cancer, Menetrier's disease, and in some cases of gastric atrophy.[15,16] Accumulation of albumin provides an abnormal molecular environment in the stomach and intestines, especially under pathological conditions. Thus, the occurrence of albumin leakage can be considered for the development of novel oral drug delivery nanocarriers.

Cubosomes are liquid crystalline lipid nanoparticles derived from lipid cubic phases, which increasingly attract interest as versatile drug delivery systems.[17–19] Liquid crystalline nanocarriers provide efficient encapsulation of bioactive molecules and improved sustained release features owing to their high surface area of both hydrophilic and hydrophobic domains within the nanoparticles.[20–25] These characteristics of the cubosomes are promising for applications in dermal, intravenous, and oral administration, especially for cancer treatments.[7,14,26–31] In the field of oral delivery, cubosomes with the surface modified

[a] Laboratory of Nano Bio Materials (LNBM), Department of Biophysics, Paulista Medical School, Federal University of Sao Paulo (UNIFESP), 04023-062 Sao Paulo, Brazil. E-mail: mertins@unifesp.br
[b] Institute of Chemistry, State University of Campinas (UNICAMP), 13083-970 Campinas, Brazil
[c] Institute of Physics, ELI Beamlines, Academy of Sciences of the Czech Republic, CZ-18221 Prague, Czech Republic
[d] Université Paris-Saclay, CNRS, Institut Galien Paris-Saclay, 91400 Orsay, France. E-mail: angelina.angelova@universite-paris-saclay.fr

with polyelectrolyte coatings have been proposed as potential carriers for transport and release of bioactive molecules in the gastrointestinal tract.[32,33]

Chitosan is a known versatile cationic biopolymer which finds diverse biomedical applications, especially as a structuring component in tissue engineering materials, thin films and in micro and nanoparticles for drug delivery.[34–36] Besides, with amino, hydroxyl and carboxyl groups in the molecular backbone, easy chemical modifications have been performed on these groups, providing specific characteristics for improvement in application purposes. In this regard, the chemical bonding of arginine on chitosan has provided improved plasmid DNA delivery for liposomes and profitable pH-responsive characteristics to micro and nanoparticles for oral drug delivery.[37–41] Additionally, alginate finds increasing application perspectives in biomedicine and food technology due to its high availability, anionic nature, and especially due to gel forming and pH-dependent properties.[42,43] As opposite charge polyelectrolytes in aqueous solutions, chitosan and alginate have been associated in the production of nanoparticles as complex coacervates intended for antibacterial, antifungal and antitumor applications.[44,45]

Recently, we have designed hybrid lipid nanoparticles of liquid crystalline structure, cubosomes, which were surface-modified with polyelectrolyte complexes, namely coacervates of the biopolymers chitosan-*N*-arginine and alginate.[32] The polyelectrolyte shells (PS) provide pH-responsive characteristics of the nanocarriers that can be highly profitable for oral administration, as demonstrated for complex coacervates.[38–41] In this study, we focus on the interaction of polyelectrolyte shell-cubosomes (PScubosomes) with serum albumin protein under pH conditions typical for the gastric and intestinal milieu. The aim is to unveil the material and physicochemical characteristics, which are significant for the development of nanoscale targeted oral drug delivery systems.

Serum albumin is a long chain polypeptide with an amino acid sequence that folds into globular structures driven by secondary intermolecular interactions. Albumin has a molecular weight of about 67 kDa and an isoelectric point (pI) around 5.0 (where pI is defined as the pH of the solution at which the net charge of the protein becomes zero).[46,47] At solution pH that is below the pI, the surface of the protein is positively charged, *i.e.*, albumin bears a net positive charge, whereas it is weakly negatively charged at pH 7.0–7.4. Under strong acid conditions, albumin adopts an extended structural conformation, whereas a compact ''heart-like'' shape is common for either basic or alkaline conditions.[48] In parallel, the charge state of the employed polyelectrolyte chains [chitosan-*N*-arginine and alginate polysaccharides] can also vary between fully ionized chains and fully deionized neutral chains associated with pH-dependent conformational changes in the same pH interval. Hence, the composition, structure and properties of the produced protein–polyelectrolyte complexes will be inherently determined by the nature and strength of the interactions between the protein and the polyelectrolyte chains in a specific environment.[49] Despite that these interactions can be primarily considered as electrostatic ones, they are further influenced by parameters such as density, distribution, patchiness, and extent of ionization of the ionizable groups on either the protein surface or the polyelectrolyte chains. Weak interaction forces, hydrophobic contributions, and conformational changes in the dispersion media can all impact the energetics of the interactions.

Here we investigate the hypothesis of whether the interactions between polyelectrolyte shell-cubosomes (PScubosomes) and serum albumin under strong acid and slightly alkaline conditions can lead to effective complexation of the protein and the nanoparticles, so that structural modifications of the latter could be advantageous for oral drug delivery applications (Fig. 1). This is a model study with regard to the complex multicomponent composition of the gut, where the role of bile salts and lipases needs to be considered as well.

## Materials and methods

### Materials

The lipid monoolein (1-oleoyl-*rac*-glycerol, 99%) and Pluronic F127 (99%) both in powder form (Sigma-Aldrich) were dissolved in chloroform at 200 and 100 mg $mL^{-1}$, respectively, as stock solutions. The polyelectrolyte chitosan-*N*-arginine (CHarg) was synthesized, purified, and characterized as previously described[40] with a degree of deacetylation of 95%, an average molecular weight ($M_W$) of 135 kDa, and a yield of 3.5% of monomers bonded to arginine. Alginate (Alg) was from Sigma-Aldrich with $M_W$ = 200 kDa and containing 61% mannuronic acid and 39% guluronic acid units. The polysaccharides were dissolved in water at 5 mg $mL^{-1}$ with overnight stirring followed by 5 min bath sonication. Bovine serum albumin (BSA, 98%) was purchased from Sigma-Aldrich. Buffers were prepared with sodium acetate and acetic acid for pH 2.0 buffer medium and disodium phosphate and citric acid for pH 7.4. All reagents were of analytical grade. Purified water was from a MilliQ system (Millipore Corp.) with a resistivity of 18 MΩ cm and a total organic carbon value of less than 15 ppb.

### Cubosome nanoparticle preparation

Cubosome dispersions were prepared following our recently described protocol[32] with monoolein (Mo) as a nonlamellar lipid, Pluronic F127 (PF127) as a dispersing agent and stabilizer, and chitosan-*N*-arginine (CHarg) and alginate (Alg) as the polyelectrolyte system, which can form charged biopolymer complexes with affinity for the intestinal mucosal membrane.[38,40] All samples were prepared in the same way with 20 mg of Mo yielding a stock lipid concentration of 135 mM. PF127 was included at 7 wt% relative to the lipid. Both Mo and PF127 were mixed in chloroform in glass vials and the solvent was evaporated under a nitrogen stream and lyophilized overnight afterwards. For preparation of blank cubosomes without biopolymer shells, pure water was added after lyophilization of the mixed films, and the samples were subjected to vortex-sonication cycles comprising 1 min vortexing and 5 min sonication 10 times. For preparation of PScubosomes with polyelectrolyte shells, the individual lipid films

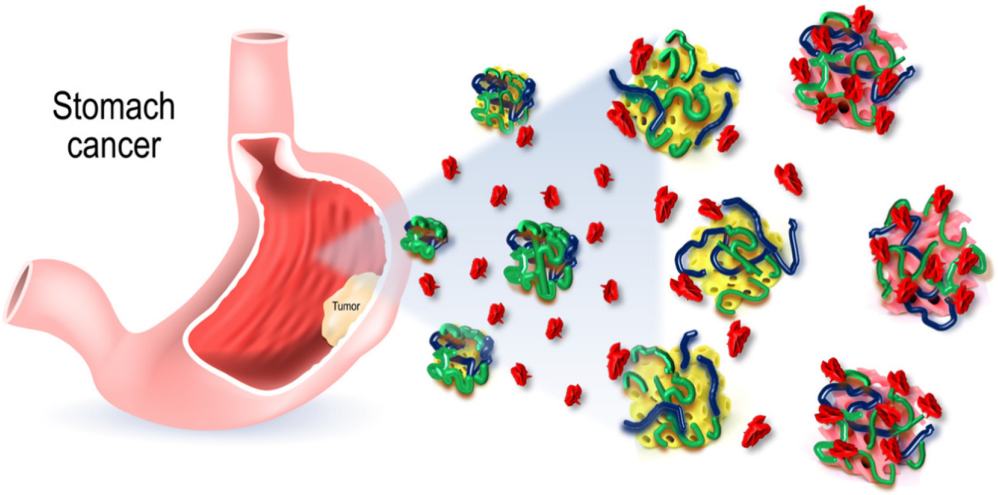


Fig. 1 Schematic presentation of drug release at the tumor site potentially provoked upon interaction of massively leaked serum albumin with orally administered polyelectrolyte shell-nanocarriers (PScubosomes). Considering that chitosan is a low digestible material, the dynamic structural effect caused by eventual digestion of the nanoparticles is not considered in this scheme. Serum albumin is present in quantity in the gut when cancerous tissue is present.

were hydrated with CHarg and Alg solutions at several different concentrations and proportions of the polyelectrolytes, providing samples with 10, 15 and 22 μM of polysaccharides and for everyone at 10, 15 or 20 wt% Alg proportion relative to CHarg. All sample volumes were adjusted to 264 μL by adding pure water when required. The vials were sealed and subjected to cycles of 10 times vortexing–sonication in an ice bath and then kept for equilibration in the dark at room temperature (22–25 °C) for one week. All samples were produced in duplicate for investigations under the two pH conditions. Subsequently, 150 μL of buffer pH 2.0 or 7.4 was added to every vial of each biopolymer concentration and each relative proportion of the polysaccharides reaching a final volume of 414 μL each. The samples were further subjected to 1 min vortexing and 5 min bath sonication and then kept at rest for one more week before structural analysis. Prior to the SAXS measurements, a volume of 100 μL of each individual dispersion was mixed with the same volume of BSA solution (10 mg $mL^{-1}$) in the corresponding buffer. For DSC the same procedure was made for the selected samples containing 22 μM of polysaccharides at 10 wt% Alg, and for this concentration an additional sample with BSA in pure water was prepared.

### Small angle X-ray scattering (SAXS)

SAXS experiments were performed at the SWING beamline[50] of Synchrotron SOLEIL (Saint Aubin, France). The sample-to-detector distance was 3 m. The patterns were recorded with a two-dimensional EigerX 4-M detector. The $q$-vector was defined as $q = (4\pi/\lambda) \sin \theta$, where $2\theta$ is the scattering angle. The synchrotron radiation wavelength was $\lambda = 1.033$ Å. The $q$-range calibration was done using a standard sample of silver behenate ($d = 58.38$ Å). The nanoparticle dispersions were filled in X-ray capillaries with a diameter of 1.5 mm and were sealed using paraffin wax. They were oriented in front of the X-ray beam (375 × 25 $\mu m^2$) using a designed holder for multiple capillary positioning ($x$, $y$, $z$). An exposure time of 1 s was used and no radiation damage was observed. The temperature was 22 °C for all samples. Selected samples containing 22 μM of polysaccharides at 10 wt% Alg were further subjected to SAXS measurements at temperatures increasing to 36, 45, 55 and 65 °C. Scattering patterns of an empty capillary, a capillary filled with MilliQ water and capillaries for each buffer solution were recorded for intensity background subtraction. Data processing of the recorded 2D images was performed by the FOXTROT software. An average of three spectra per capillary was acquired at two positions along the capillary length.

The lattice parameters ($a$) of the liquid crystalline phases were derived from the Bragg peaks detected in the X-ray diffraction patterns. The assigned reflections were fitted through the Miller indexes according to the relation:

$$q = (2\pi/a)\,(h^2 + k^2 + l^2)^{1/2} \quad (1)$$

from linear fits of the plots of $q$ *versus* $(h^2 + k^2 + l^2)^{1/2}$, where $q$ is the peak position along the scattering vector axis and $h$, $k$, and $l$ are the Miller indexes of the respective cubic lattice. The slope of the linear fit to the data equals the inverse of the cubic lattice parameter.[51]

### Quasi-elastic light scattering and zeta potential

Quasi-elastic light scattering (QELS) and zeta potential measurements were performed with Nano-ZS90 Malvern ZetaSizer equipment (Malvern Instruments, UK) operating with a 4 mW HeNe laser at a wavelength of 632.8 nm in a temperature-controlled chamber at 25 °C. Aliquots of the cubosome dispersions were diluted with 1 mL of pure water or the corresponding buffer, in which the individual sample was prepared. BSA solutions under the same conditions were at 1 mg $mL^{-1}$.

 

QELS measurements were made with the samples in cuvettes and scattering was acquired at an angle of 90°. The typical autocorrelation function was obtained using exponential spacing of the correlation time. The data analyses were performed with software provided by Malvern. The intensity-weighted size distribution was obtained by fitting data with a discrete Laplace inversion routine. Size determination was made using a Stokes–Einstein relation and the polydispersity was accessed by using cumulant analysis of the correlation functions measured by QELS applying the amplitude of the correlation function and the relaxation frequency. The second-order cumulant was used to compute the polydispersity of samples. Each analysis was a result of three consecutive measurements. The colloidal size was expressed as hydrodynamic diameter.

Zeta potential was measured in the same equipment using the folded capillary zeta cell and changing the detection angle to 173°. Data were acquired performing at least 100 runs per sample. The principle of the measurement is based on laser Doppler velocimetry. The electrophoretic mobility was converted to zeta potential using the Helmholtz Smoluchowski relationship and the data were obtained in mV.

### Differential scanning calorimetry

DSC scans were performed in a Microcal PEAQ-DSC Microcalorimeter (Microcal Inc., Northampton, MA, USA) equipped with 0.13 mL twin total-fill cells. The reference cell was filled with water or buffer and the sample cell with 10 mg $mL^{-1}$ BSA in water or buffers with and without cubosomes. Samples were heated from 20 to 90 °C using a heating ramp of 1 °C $min^{-1}$. Scans were performed at least in duplicate.

### Isothermal titration calorimetry

The ITC measurements were performed in a VP-ITC microcalorimeter (MicroCal Inc., Northampton, MA). Before the measurements, all samples were degassed for 5 min under reduced pressure in order to avoid the interference of air bubbles in the aqueous suspensions. Following the standard procedure, the working cell of 1.4576 mL in volume was filled with 0.3 mM BSA solution dissolved in the same buffer solutions as cubosome dispersions. One aliquot of 2 μL followed by 27 aliquots of 10 μL of the cubosome or PS-cubosome suspension in the same buffer were injected stepwise with a 400 s interval into the working cell. The sample cell was constantly stirred (307 rpm), and the experiments were performed at 37 °C. The data acquisition and analyses were carried out with Origin software provided by MicroCal. The data fitting was performed applying the single set of identical binding sites model, as previously described, using a non-linear least square fitting.[52] Briefly, the binding constant $K$ is defined as:

$$K = \theta/(1 - \theta)\, C_{\text{free}} \quad (2)$$

where $\theta$ = [bound monoolein]/$N[L]$ is the fraction of BSA "bound" to monoolein on cubosomes, $[L]$ is the total concentration of BSA, and the number of binding sites $N$ represents the number of monoolein bound to BSA at saturation of binding sites. In eq. 2, $C_{\text{free}}$ is the concentration of free ("unbound") monoolein as:

$$C_{\text{free}} = C_{\text{tot}} - N\theta[L] \quad (3)$$

where $C_{\text{tot}}$ is the total monoolein concentration. The combination of eqn (2) and (3) provides a quadratic equation for the molar fraction $\theta$, and by solving this equation, one gets an expression for $\theta$ as a function of BSA concentration. Thereafter, the heat release per injection, $\delta Q$, where the bound fraction changes by $\delta\theta$, is:

$$\delta Q = N[L]V\Delta H\delta\theta \quad (4)$$

with $V$ the volume in the sample cell and $\Delta H$ the molar enthalpy. By fitting the measured heat release $\delta Q$ with this expression, the fitting parameters $N$, $K$, and $\Delta H$ are determined.

## Results and discussion

### Protein BSA zeta potential and structural transitions as a function of solution pH

Table 1 shows the hydrodynamic diameters, $d_H$, and zeta potential values for BSA in solutions with two pH values investigated in this study. An average $d_H$ of 10.1 nm was determined at pH 2.0, and $d_H$ = 6.4 nm at pH 7.4, and $d_H$ = 6.1 nm were measured in pure water for comparison. The size increment at acidic pH suggested unfolding of the BSA structure in the medium below the isoelectric point (pI around 5.0). It is known that the BSA macromolecules adopt different solution conformations, which are dependent on the changes in pH and ionic strength.[53] In their normal conformation, the albumin molecules resemble a heart shape and consist of 3 main domains and 6 sub-domains generating α-helical patterns.[48] The albumin isomeric forms at different pH values correspond to different α-helical contents. The structural conformers have been classified as normal (N), fast migration (F), and extended (E) states. In the pH range of 4–9, the N conformer of BSA was found to be 8.3 nm in length. However, at pH values lower than 4.5, the BSA molecules assume a more extended shape and may reach apparent lengths between 18.1 nm (at pH 4.0) and 26.7 nm (at pH 3.0).[53] At pH 2.7, BSA has been characterized as an oblate spheroid with dimensions 2.1 × 2.1 × 25.0 nm.[54] Hence, the extended conformation of BSA is predominant in a strong acid environment. Thus, the size results in Table 1 appear to be in accordance with the current interpretation of the BSA solution structure.

Table 1 Hydrodynamic diameters, $d_H$, and zeta potential values of BSA (1 mg $mL^{-1}$) in buffer solutions and pure water

| Solution | Hydrodynamic diameter (nm) | PDI[a] | Zeta potential (mV) |
|---|---|---|---|
| pH 2.0 | 10.1 ± 5.7 | 0.36 | 11.6 ± 4.6 |
| pH 7.4 | 6.4 ± 1.5 | 0.28 | −5.5 ± 3.5 |
| Water | 6.1 ± 2.8 | 0.37 | −23.7 ± 6.1 |

[a] Size polydispersity index.

The known isoelectric point between 4.8 and 5.1 implies that BSA acquires a positive charge at pH below 5.[46,47] The charge increases monotonically with the decrease in pH. On the other hand, the net negative charge increases at pH over 5. Thereby, self-aggregation of BSA is not expected under both studied conditions, *i.e.*, at pH 2.0 and pH 7.4. In analyzing the sizes and the size distributions in terms of hydrodynamic diameters ($d_H$) (Table 1), one can deduce that no aggregation of BSA was produced in the studied aqueous solutions.

The zeta potential data with average values of 11.6 mV at pH 2.0 and −5.5 mV at pH 7.4 indicated a less expressive pH-variation of the zeta potential as compared to previous studies.[55] Because the BSA molecule is characterized by an asymmetric charge distribution, created by both acid and basic amino acids, the magnitude of the zeta potential appears to be dependent on the conformational exposure of the acid or basic residues. The latter ionizes depending on the solution characteristics such as pH and ionic strength. Therefore, the variations of BSA zeta potential should be considered with caution, further taking into account that the protein unfolding in acid medium, with a consequent size increase, also leads to prominent distribution of charges along the extended structure. Thus, the electrical charge density may be smaller than expected. Indeed, the determined zeta potential close to neutrality for BSA in buffers is liable to the specific characteristics of the solutions. It is noted that the obtained average zeta potential of −23.7 mV in pure water indicates the predominance of BSA negative surface charge under low ionic strength conditions.

### Thermodynamic interactions in BSA-cubosome dispersions

**Differential scanning calorimetry.** The DSC profiles of BSA solutions are shown in Fig. 2a for pH 2.0, 7.4, and in purified water as a reference (*i.e.*, absence of salts). At pH 2.0 and in purified water, the observed endothermic transitions were broad, with a positive value for the heat capacity change. The transition temperature $T_m$ (defined as the temperature at which a local maximum occurs in the excess heat capacity) was lower for the pH 2.0 solution, with a maximum at 42.4 °C (Table 2). This result evidences that the BSA transition in acidic solution occurs at lower temperature. The shape of the curves corresponding to BSA denaturation differs essentially. The highly broad curve along with the lower $\Delta H$, compared to the other solutions, suggests that the transition of the extended structure of BSA in strong acid medium is less cooperative and requires reduced thermal energy.

Table 2 DSC results for transition temperature ($T_m$, °C), enthalpy variation ($\Delta H$, kcal mol$^{-1}$), and entropy variation ($\Delta S$, kcal mol$^{-1}$ K$^{-1}$) for BSA under the studied conditions

| BSA | | | | BSA + cubosomes | | | BSA + PScubosomes | | |
|---|---|---|---|---|---|---|---|---|---|
| Solution | $T_m$ | $\Delta H$ | $\Delta S$ | $T_m$ | $\Delta H$ | $\Delta S$ | $T_m$ | $\Delta H$ | $\Delta S$ |
| pH 2.0 | 42.4 | 23.2 | 0.074 | 54.3 | 27.4 | 0.083 | 47.7 | 1.1 | 0.003 |
| pH 7.4 | 60.2 | 193.1 | 0.579 | 65.5 | 160.0 | 0.473 | 76.6 | 126.2 | 0.361 |
| Water | 57.6 | 121.8 | 0.368 | 67.5 | 117.0 | 0.344 | 81.5 | 91.6 | 0.258 |

In purified water, the DSC curve shifted and $T_m$ of 57.6 °C was obtained and the curve with increased $\Delta H$ showed an apparent right shoulder. In buffer with pH 7.4, $T_m$ was close to 60.2 °C, but a narrowed peak of higher intensity, depicting a further $\Delta H$ increase, evidences that the normal compact conformational structure of BSA requires higher thermal energy for the transition. The obtained results show that ionic strength and buffer pH play a crucial role in providing a more cooperative transition, which led to a narrow peak.

The comparison with the same BSA solutions containing blank cubosomes (Fig. 2b) evidenced that $T_m$ increases for all conditions (Table 2). In parallel, $\Delta H$ slightly increases at pH 2.0, but decreases in water, and more significantly decreases to 160 kcal mol$^{-1}$ at pH 7.4. For BSA solutions containing PScubosomes (Fig. 2c), $T_m$ was further increased at pH 7.4 and in water, with a concomitant $\Delta H$ decrease under both conditions. The endothermic curve almost vanished for the pH 2.0 condition and a remaining discrete signal is noticed at 47.7 °C (Table 2). This steep decrease of $\Delta H$ suggests that the forces, which maintain the conformation of BSA molecules, are weakened by the presence of blank cubosomes and PS-cubosomes. Instead, higher thermal energy is necessary for the transitions.

It is known that the thermal denaturation of proteins comprises two steps. One is the unfolding process, which is endothermic, and in most cases reversible, and the other is the subsequent aggregation or precipitation of denatured proteins, being exothermic and irreversible.[56,57] Thereby, the experimental $\Delta H$ value is the sum of the heat of unfolding and the

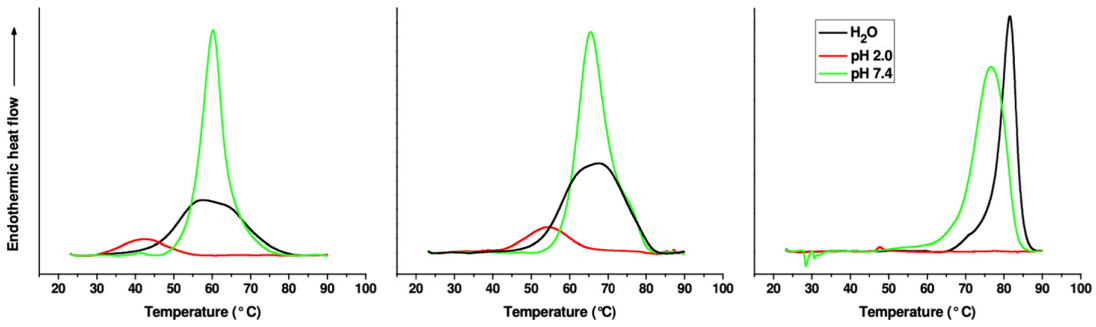


Fig. 2 DSC curves for BSA in solution (a) and BSA incubated with blank cubosomes (b) and PScubosomes (c) at the same pH values of the environment.

 

Table 3 Thermodynamic parameters characterizing the interaction of PScubosomes (a) and blank cubosomes (b) with BSA protein at 37 °C under the studied pH conditions

| pH | $N$ | $K$ ($10^4$ $M^{-1}$) | $\Delta H$ (kcal $mol^{-1}$) | $\Delta G$ (kcal $mol^{-1}$) | $\Delta S$ (kcal $mol^{-1}$ $K^{-1}$) |
|---|---|---|---|---|---|
| 2.0 | 2.51 ± 0.04 | 2.39 ± 0.29 | −1.085 ± 0.025 | −8.689 | 0.024 |
| 7.4 | 0.65 ± 0.11 | 0.24 ± 0.04 | −3.485 ± 0.711 | −7.275 | 0.012 |
| 2.0 | * | * | ∼(0.270) | * | * |
| 7.4 | * | * | ∼(-0.425) | * | * |

Number of binding sites, $N$; binding constant, $K$; molar enthalpy, $\Delta H$; Gibbs energy, $\Delta G$; entropic contribution, $\Delta S$.

heat of aggregation. In the presence of blank cubosomes and PScubosomes, the possible interaction with the nanoparticles belongs thus to the second step. Thereby, the interaction contributes to an exothermic process hence reducing the effective $\Delta H$ as shown in Table 3. Furthermore, the decrease in $\Delta H$ is more significant in the presence of PScubosomes, suggesting that the interaction with BSA is indeed stronger with these nanoparticles. These observations are further confirmed with ITC, as discussed in the following section. In terms of $\Delta S$ (determined as $\Delta S = \Delta H/T_m$), a consistent decrease is shown in Table 2 compared to BSA alone, and the presence of blank cubosomes and PScubosomes for all conditions. These results unveil that thermal transitions of BSA are affected in the presence of blank cubosomes and much more in the presence of PScubosomes. It is suggested that BSA shows no apparent transition at pH 2.0 in the presence of PScubosomes. Overall, BSA displays higher thermal stability in mixtures with PScubosomes.

**Isothermal titration calorimetry.** The effective thermodynamic interaction between the cubosomal dispersions and BSA was studied by titration under controlled conditions with ITC. It was found that polyelectrolyte-free (blank) cubosomes show weak interactions with BSA. Besides, the thermodynamics of this weak interaction was absolutely opposite when comparing the strong acid media with the slightly alkaline one as shown in Fig. 3.

At pH 2.0, a clear endothermic heat was unveiled at every titration of blank cubosomes into BSA solution (Fig. 3a), leading to an average $\Delta H$ of ∼0.270 kcal $mol^{-1}$ (Table 3). At pH 7.4, the weak BSA–cubosome interaction was clearly exothermic for all investigated titrations (Fig. 3b), typically with $\Delta H$ in the order of −0.425 kcal $mol^{-1}$. No saturation of titration was found at both pHs in a range of concentrations. For the extended conformation of BSA at pH 2.0,[54] the endothermic heat may be associated with the sum of the conformational change of BSA (when coming in contact with the cubosome), besides breaking of H bonds in BSA, and the formation of new H bonds of BSA at the surface of cubosomes (containing Mo polar heads and Pluronic F127 chains). For the globular structure of BSA at pH 7.4,[53] the interaction with the blank cubosomes was probably not leading to conformational changes, but rather to water release from the entangled globular proteins. Besides, the formation of hydrogen bonds with the cubosome surface provided exothermic heat. In sum, the absorbed or released heat at pH 2.0 and pH 7.4, respectively, should correspond to weak interactions which do not lead to effective complexation of BSA with the blank cubosomes. Indeed, the intensity of the heat at every new injection of cubosomes was close to the intensity of the heat of all previous injections, and thus no saturation was achieved (Fig. 3a and b).

Dramatically different results were obtained for polyelectrolyte-shell PScubosomes. Fig. 3c and d show that heat was released upon interaction with BSA at both pH 2.0 and 7.4. This evidenced a clear exothermic interaction, which reached effective saturation during titration. It is noted that for a Mo/BSA molar ratio over 2 at pH 2.0, the exothermic heat is preceded by increasing endothermic heat, which increased to a constant intensity after

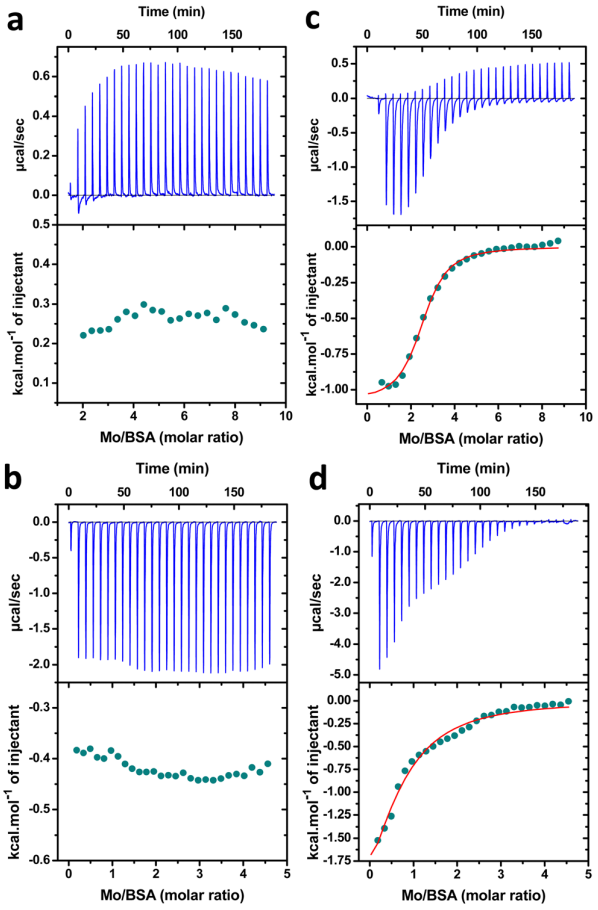


Fig. 3 ITC results for the titration of blank cubosomes (left) and PS-cubosomes (right) in BSA (0.3 mM) at 37 °C, all in pH 2.0 (a and c) and 7.4 (b and d) buffers. The solid red curves are fits according to the model for one set of binding sites after subtraction of the heats of dilution.

the exothermic heat vanished. The exothermic heat can be attributed to the effective interaction of BSA with the PScubosomes. Comparing Fig. 3a with Fig. 3c, the intensities of the endothermic heat in the two independent experiments were roughly similar. However, the endothermic heat in the experiment with the PScubosomes may predominantly arise from the interaction of PScubosomes with PScubosomes which already contain BSA coordinated on their surface during the previous injection.

The effective interaction between PScubosomes and BSA led to a change of $\Delta H$ of $-1.085$ kcal mol$^{-1}$ at pH 2.0 and $-3.485$ kcal mol$^{-1}$ at pH 7.4 (Table 3), which suggested stronger interaction under the latter condition. For the achieved saturation in the titrations with PScubosomes, it was possible to fit the data applying a single set of binding sites,[52] hence providing complete thermodynamic profiles (Table 3). The magnitude of the equilibrium constant $K$ represented favored interactions in both media. Additionally, the number of binding sites $N = 0.65$ at pH 7.4 and $N = 2.51$ in strong acids indicated that the Mo/BSA ratio is considerably higher at pH 2.0. This pointed out that less BSA was effectively interacting with the particles at pH 2.0. These results evidenced that a higher amount of BSA strongly interacts with the PScubosome at pH 7.4.

In terms of $\Delta G$ (calculated applying $\Delta G = -RT\ln(55.55\ \text{K})$, where $\Delta G$ is defined for the standard state of mole fraction, $T$ is the temperature, and 55.55 introduces the concentration of water),[52] the results further evidenced a favored thermodynamic interaction with prominent reduction in Gibbs energy under both conditions (Table 3). Intriguingly, the positive entropic contributions, two times higher at pH 2.0, suggested expansion of the interacting system. This may arise from any kind of conformational changes in the involved components, counter ions and water molecules released from both nanoparticles and BSA, redistribution of the hydrogen bond network or the van der Waals interactions. Specifically at pH 7.4, a hydrophobic contribution of deprotonated chitosan chains over the surface of the PScubosome should not be excluded.

### Structural features of BSA interactions with PScubosomes *versus* blank-cubosomes

The obtained SAXS results on the interaction of biopolymer (chitosan-*N*-arginine/alginate)-functionalized lipid nanoparticle dispersions with albumin at different pH values are presented and discussed considering (i) the inner liquid crystalline nanochannel network organization of the generated self-assembled cubosome nanoparticles and their capacity to entrap protein species under different environmental conditions impacting the hydration of the molecules; (ii) the possible electrostatic complexation between the cubosome nanoparticles that exhibit pH-dependent surface charge (determined by the chitosan-*N*-arginine-to-alginate ratio referred to as CHarg/Alg) and the protein biomolecules of different ionization states and/or conformation; and (iii) albumin binding on the nanoparticle surface in the shape of a protein corona dependent on pH.

Fig. 4 shows the SAXS patterns acquired upon incubation and assembly of biopolymer-functionalized (Mo/PF127/CHarg/Alg) lipid nanoparticles and albumin at pH 2.0 and 7.4. The detected Bragg diffraction peaks in the patterns identify cubic liquid crystalline inner organization of the investigated nanoassemblies and confirm the formation of cubosome structures. The upper dark blue plot indicates that the incubation of albumin with blank (Mo/PF127) cubosomes, which lack a surface coverage by polysaccharide (CHarg/Alg) shells, does not modify the inner primitive *Im3m* cubic lattice organization typical for the Pluronic F127-stabilized Mo cubosomes (see also the structural parameters reported for pure Mo in Table 2 of ref. 32). Indeed, the cubic lattice spacing ($a_{Im3m}$ = 13.65 nm) determined after the nanoparticle mixing with albumin does not significantly differ from that of the blank Mo/PF127 cubosomes ($a_{Im3m}$ = 13.9 nm) at pH 2.0. This confirms weak interaction between the neutral cubosome Mo lipid nanoparticles and the positively charged protein. The result agrees with the ITC data. The hydration of the inner primitive-type *Im3m* cubic lattice network appears to be slightly decreased. At pH 7.4, the interaction of the blank Mo/PF127 cubosomes with the protein remains weak as deduced from the obtained cubic unit cell parameter $a_{Im3m}$ = 13.59 nm, which slightly differs from $a_{Im3m}$ = 12.80 nm obtained for the same nanoparticles in the absence of albumin.[32]

At variance to the neutral blank Mo/PF127 cubosomes which lack biopolymer shells, the interaction of the polysaccharide-functionalized (Mo/PF127/CHarg/Alg) lipid dispersions with the protein resulted in notable structural changes in the PScubosome nanoparticles. As shown in Fig. 4, the obtained SAXS curves evidence new Bragg diffraction peaks for the PScubosomes for all studied concentrations and relative proportions of the polysaccharides.

The indexing of the SAXS patterns revealed the occurrence of coexistence of two distinct cubic symmetries corresponding to the initial *Im3m* and a new *Pn3m* phase. The lattice parameters are depicted in Table 4 showing a reproducible partial phase transition for almost all samples. At pH 2.0, the lattice parameter varied between 13.47 and 14.02 nm for the *Im3m* cubic structure and between 10.11 and 10.55 nm for the *Pn3m* cubic phase, without an apparent tendency relative to the biopolymer concentrations. However, at pH 7.4, the lattice parameter varied between 13.77 and 16.42 nm for the *Im3m* cubic structure and between 10.08 and 11.87 nm for the *Pn3m* cubic phase. This result denoted a slight increase of the internal repeat distances for both phases with the increase of the biopolymer concentration and also with an increase of the Alg relative proportion. It is noted that the sample containing 22 μM biopolymers at 10% Alg showed the sole occurrence of inner *Im3m* cubic symmetry. The intensities of the Bragg reflections at pH 7.4 for the majority of the samples in 15 and 22 μM of biopolymers, and specially for the 20% Alg, were low and broad. Overall, these results suggested a stronger interaction of the PScubosomes with albumin at pH 7.4, and confirmed the thermodynamic studies.

As illustrated in Fig. 5, the established partial phase transition is suggested to result from effective nanoparticle–protein interactions, which are promoted by the biopolymer shells.

 

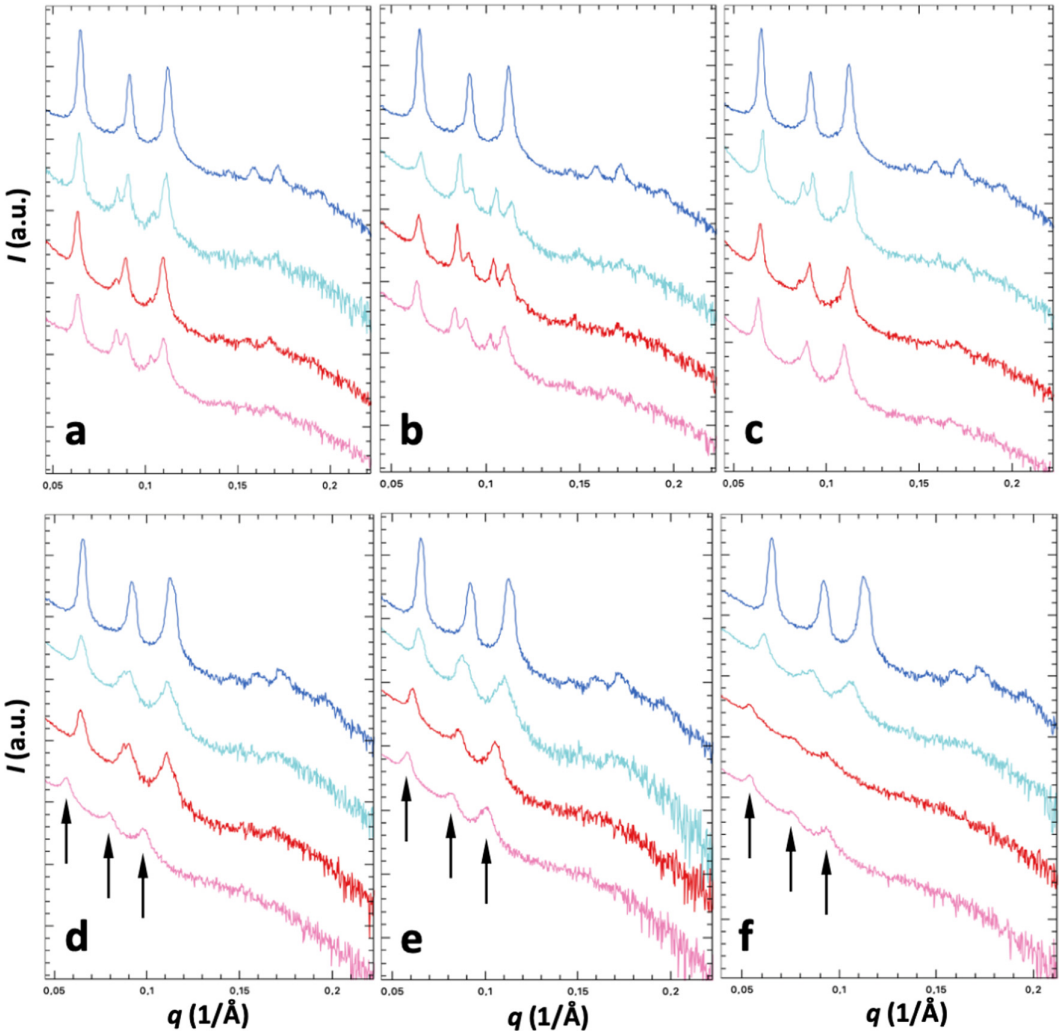


Fig. 4 SAXS patterns recorded after cubosome-BSA incubation at pH 2.0 (a–c) and 7.4 (d–f). Higher curves: blank cubosomes (Mo + PF127) in BSA as a reference system (dark blue), and from up to down: PScubosomes (Mo + PF127 + CHarg + Alg) in the BSA environment with increasing concentration of PS polyelectrolytes (10, 15, and 22 μM): (a and d) 10 wt% Alg. (b and e) 15 wt% Alg. (c and f) 20 wt% Alg. Arrows in the lower panels indicate the positions of the Bragg peaks resolved for the low intensity curves. The reader is referred to Table 4 for the classification of the PScubosome compositions containing 3 concentrations of polyelectrolytes (μM) for 3 relative proportions of Alg (wt%).

Actually, the phase transition from *Im*3*m* to *Pn*3*m* cubic lattice organization requires an increase in the curvature of the lipid bilayers in the cubic network (Fig. 5), which leads to the reduction of the lattice parameter (as described above). Such a phase transition occurring in the presence of albumin may have implications for the *in vivo* performance of the nanocarriers, considering that changes in the bilayer curvature and a decrease of the internal spaces of the cubic network represent structural features that may promote effective release of encapsulated bioactive molecules. Indeed, the transition to *Pn*3*m* may lead to the squeezing out of hydrophilic compounds due to the dehydration resulting from the cubic lattice distance reduction.[58] Besides, the increase of the lipid bilayer curvature may provide higher exposure of hydrophobic compounds entrapped in the cubosomes, thus facilitating their release when reaching the cellular membranes.

The stability of the Mo/PF127/CHarg/Alg cubosomes incubated with albumin at pH 2.0 and 7.4 was investigated in the temperature range from 22 to 65 °C (Fig. 6) for the selected samples containing 22 μM of biopolymers at 10 wt% Alg. These samples were selected considering the greater difference in the zeta potential of the nanoparticles at pH 2.0 with 7.4 (Table 4), in the range of 18.0 mV and −39.0 mV, respectively, on the average. The SAXS patterns clearly show, with increasing temperature, the occurrence of phase transitions accompanied by splitting of the Bragg diffraction peaks at pH 2.0 (Fig. 6a). These data indicated the induction of two liquid crystalline structures in the mixed lipid/biopolymer/protein systems studied at pH 2.0.

Table 4 Lattice parameters for the indicated cubic symmetry of PScubosomes containing 3 concentrations of polyelectrolytes (μM) for 3 relative proportions of Alg (wt%), all samples in excess of BSA. Zeta potential for the PScubosomes before incubation in BSA

| 10% Alg | 10 μM | | | 15 μM | | | 22 μM | | |
|---|---|---|---|---|---|---|---|---|---|
| pH | *Im3m* (nm) | *Pn3m* (nm) | Zeta (mV) | *Im3m* (nm) | *Pn3m* (nm) | Zeta (mV) | *Im3m* (nm) | *Pn3m* (nm) | Zeta (mV) |
| 2.0 | 13.75 | 10.27 | 4.95 ± 4.06 | 14.02 | 10.54 | 8.35 ± 4.69 | 13.97 | 10.49 | 18.0 ± 6.01 |
| 7.4 | 13.82 | 10.12 | −23.4 ± 4.07 | 13.77 | 10.08 | −21.3 ± 3.62 | 15.67 | — | −39.0 ± 3.30 |
| 15% Alg | 10 μM | | | 15 μM | | | 22 μM | | |
| pH | *Im3m* (nm) | *Pn3m* (nm) | Zeta (mV) | *Im3m* (nm) | *Pn3m* (nm) | Zeta (mV) | *Im3m* (nm) | *Pn3m* (nm) | Zeta (mV) |
| 2.0 | 13.47 | 10.32 | 2.63 ± 3.81 | 13.72 | 10.44 | 6.72 ± 4.07 | 13.93 | 10.55 | 10.6 ± 5.23 |
| 7.4 | 13.89 | 10.12 | −21.1 ± 3.72 | 14.50 | 10.43 | −23.8 ± 3.09 | 15.14 | 11.08 | −25.6 ± 4.74 |
| 20% Alg | 10 μM | | | 15 μM | | | 22 μM | | |
| pH | *Im3m* (nm) | *Pn3m* (nm) | Zeta (mV) | *Im3m* (nm) | *Pn3m* (nm) | Zeta (mV) | *Im3m* (nm) | *Pn3m* (nm) | Zeta (mV) |
| 2.0 | 13.50 | 10.11 | 1.64 ± 4.11 | 13.74 | 10.33 | 3.63 ± 9.26 | 13.98 | 10.46 | 3.77 ± 5.75 |
| 7.4 | 14.46 | 10.90 | −22.5 ± 6.58 | 16.42 | 11.87 | −18.7 ± 6.65 | 16.38 | 11.85 | −24.4 ± 3.26 |

Zeta variations (±) are standard deviations obtained from the respective experiment.

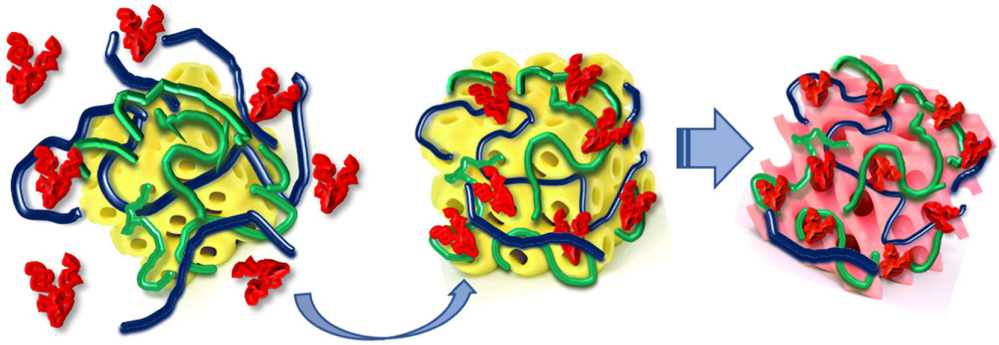

Fig. 5 Schematic representation of the BSA protein (red structures) interacting with the biopolymer shells (blue and green structures) on the PScubosomes leading to complexation of BSA over the nanoparticles and a transition from *Im3m* (yellow) to *Pn3m* (rose) cubic symmetry of the nanocarrier liquid crystalline organization.

Starting from room temperature, the Bragg peaks of the primitive *Im3m* cubic lattice cubosomes were present in the SAXS patterns of the Mo/PF127/CHarg/Alg formulations at all temperatures upon heating up to 65 °C. The inner cubic unit cell lattice parameter ($a_{Im3m}$ = 13.97 nm) of the cubosomes determined at 22 °C (Table 4) is close to that of the pure MO/PF127 cubosomes at pH 2.0 ($a_{Im3m}$ = 13.9 nm) previously reported.[32] Interestingly, Bragg peaks of a second cubic phase structure were also detected in the SAXS curves of the dispersed lipid/biopolymer/protein (Mo/PF127/CHarg/Alg/BSA) assemblies upon increasing temperature. They were fitted by the coexisting reflections of a primitive *Im3m* and double diamond *Pn3m* types of cubic phases and the determined lattice parameters are presented in Table 5. The formation of the *Pn3m* cubic structure can be attributed to the partial entrapment of protein biomolecules within the PScubosome particles. Such a coexistence of *Im3m* and *Pn3m* cubic lattice structures has been already reported for lipid/peptide cubosome systems at partial peptide loading that occurs at low peptide concentrations[23] and in lipid/chitosan hydrogels.[59]

The obtained SAXS results further suggested that the concentration of the protein molecules in the aqueous phase is insufficient to entirely transform the *Im3m* cubic structure of the Mo/PF127/CHarg/Alg cubosome particles into the *Pn3m* cubic symmetry. It should be noted that high BSA concentrations, that could result in higher protein loading, leads to precipitation of big aggregates and the impossibility to investigate dispersed Mo/PF127/CHarg/Alg/BSA assemblies. Therefore, the concentration investigated here was chosen as to correspond to aqueous dispersions of cubosomal objects, which are stabilized by repulsive forces between their functionalized surfaces.

The lattice parameters of the *Im3m* and *Pn3m* cubosome structures presented in Table 5 were found to decrease with increasing temperature. This result can be explained by the temperature effect on the membrane curvature and the dehydration of the lipid/water interfaces in the three-dimensional network membrane organization.[58] Heating from 36 °C to 65 °C leads to progressive squeezing of water molecules from the cubosomal nanochannels, which results in dehydration of the inner liquid crystalline organization of the nanoparticles.

 

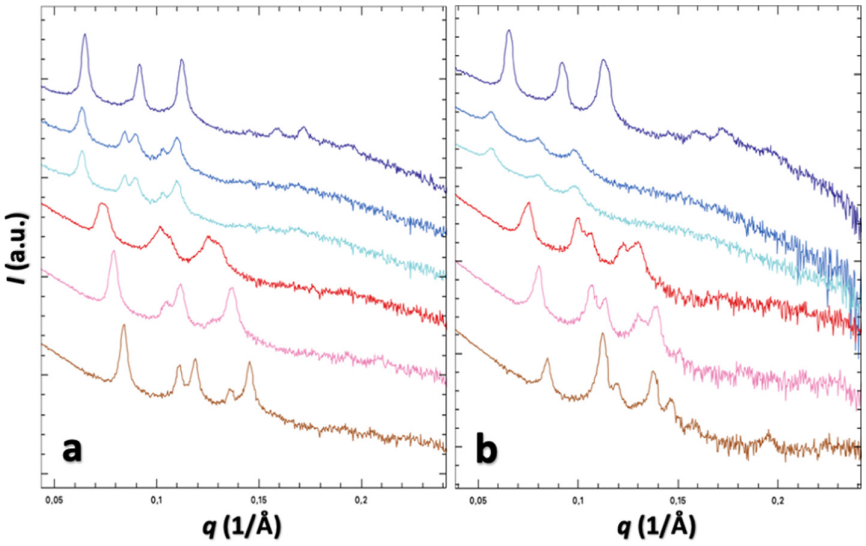


Fig. 6 SAXS patterns of blank and PScubosomes at varying temperatures. Higher curve (dark blue): blank cubosomes (Mo/PF127) in albumin as a reference sample; from up to down: PScubosomes (Mo/PF127/CHarg/Alg) with 22 μM biopolymers/10 wt% Alg, in BSA solution at temperatures 22, 36, 45, 55 and 65 °C. (a) pH 2.0. (b) pH 7.4.

Table 5 Lattice parameters of PScubosome dispersions (22 μM biopolymers – 10 wt% Alg) in BSA solution for the indicated cubic symmetries as a function of temperature

| Temperature (°C) | *Im3m* (nm) | *Pn3m* (nm) |
|---|---|---|
| pH 2.0 | | |
| 22 | 13.97 | 10.49 |
| 36 | 14.00 | 10.51 |
| 45 | 12.25 | 8.40 |
| 55 | 11.21 | 8.46 |
| 65 | 10.55 | 8.01 |
| pH 7.4 | | |
| 22 | 15.67 | — |
| 36 | 15.64 | — |
| 45 | 11.80 | 8.89 |
| 55 | 11.02 | 8.34 |
| 65 | 10.48 | 7.90 |

Correspondingly, the cubic lattice parameters decrease from $a_{Im3m}$ = 14.0 nm to 10.55 nm and from $a_{Pn3m}$ = 10.51 nm to 8.01 nm (Table 5). Notably, both *Im3m* and *Pn3m* cubic symmetries were preserved (Fig. 6a).

Fig. 6b presents the SAXS patterns characterizing the interaction of the Mo/PF127 and Mo/PF127/CHarg/Alg self-assembled liquid crystalline nanoparticles with albumin at pH 7.4. The interaction of the blank Mo/PF127 cubosomes with the protein also remains weak at pH 7.4 as deduced from the obtained cubic unit cell parameter $a_{Im3m}$ = 13.59 nm, which slightly differs from the value $a_{Im3m}$ = 12.80 nm, obtained for the same nanoparticles in the absence of albumin.[32] However, notable structural changes are straight distinguished for the Mo/PF127/CHarg/Alg assemblies with regard to the pH 2.0 condition. First, the intensity of the Bragg diffraction peaks of the *Im3m* cubic lattice decreases upon increasing the temperature from 22 °C to 65 °C. The phase transition from the *Im3m* to the *Pn3m* cubic phase structure occurs gradually upon heating the aqueous dispersion at pH 7.4 and the latter was clearly identified at 45 °C (Table 5). Second, the Bragg diffraction peaks corresponding to the *Pn3m* cubic phase possessed noticeable higher intensity compared to the *Im3m* structure, especially at 65 °C (Fig. 6b). These outcomes are essentially different from those presented in Fig. 6a.

It can be inferred from the data in Fig. 6b and Table 5 that the *Im3m* cubic phase structure undergoes a temperature-induced destabilization, which is favored by the dehydration of the aqueous channels in the inner organization of the nanoparticles.[58] Correspondingly, the Bragg peak intensities of the diamond cubic *Pn3m* lattice increase. Moreover, the hydrophobic and charge–charge interactions between the weakly negatively charged BSA molecules at pH 7.4 and the lipid cubosomes with polysaccharide (CHarg/Alg) shells appear to contribute to the overall dehydration of the Mo/PF127/CHarg/Alg/BSA assemblies, and thus to the *Im3m* cubic phase destabilization. The SAXS plots in Fig. 6b (from top to bottom) clearly show that the transition to a less hydrated *Pn3m* mesophase cubic structure is favored by increasing the temperature from 45 °C to 65 °C. The temperature dependences of the determined $a_{Im3m}$ and $a_{Pn3m}$ cubic lattice parameters of the Mo/PF127/CHarg/Alg/albumin self-assembled supramolecular structures are presented in Table 5 showing a consistent decrease with an increase in temperature, similar to the pH 2.0 condition. Whereas the population of *Im3m* cubosomes was essentially diminished at pH 7.4 (in comparison to that at pH 2.0), the growing Bragg peak intensities of the less hydrated *Pn3m* cubic lattice at pH 7.4 suggested that the interaction between the protein and the PScubosomes, besides the phase transition, led to expulsion of water from the aqueous nanochannel networks present inside the nanoparticles.

## Conclusions and perspectives

The interaction of serum albumin with conventional blank monoolein-Pluronic F127 cubosomes was found to be weak in terms of thermodynamics and no notable structural changes in the nanoparticle liquid crystalline structure were observed. At variance, strong interaction between serum albumin and polyelectrolyte shell-cubosomes (PScubosomes) was evidenced by the observed enthalpic, entropic and Gibbs energy variations under simulated gastric and intestinal pH conditions. The ITC results indicated that the interactions at both pH values are not purely electrostatic. The effective PScubosome–protein interaction led to alteration of the internal cubic lattice symmetry of the particles and a partial transition from the original *Im3m* cubic structure to *Pn3m* structure characterized by a higher lipid membrane curvature. Furthermore, a decrease of the internal cubic lattice spacings of both *Im3m* and *Pn3m* cubosomes provided evidence for the reduction of the internal water channels, and thus water squeeze was provoked by the protein. These characteristics may trigger release of encapsulated bioactive molecules upon PScubosome complexation with serum albumin under gastrointestinal cancerogenic conditions. In perspective, the concept presented here can be applied to oral delivery of various anticancer drugs by PScubosome nanocarriers.

In general, there is still a relatively poor understanding of how real gastrointestinal conditions affect the physicochemical characteristics of nanoparticles.[60] The presence of bile salts in the gut may have dramatic structural effects on the lipid carriers if they display a propensity for the formation of mixed micelles. However, the polysaccharide shells on the surface of the cubosomes studied here may provide an improved structural stability when considering the reported fact that chitosan is a low digestible polysaccharide. Besides, the pH-responsive surface charge provided by the cationic and anionic polysaccharides may inhibit the lipase action and influence the digestibility effect of bile salts as well as.[61] In terms of gastrointestinal cancer, the albumin presence in the gut represents an additional component which can lead to corona formation on nanocarriers and yield structure variation, depending on the strength of interaction as shown in this study. The understanding of these processes provides important insights into the design of nanoparticle-based delivery systems that are highly effective and safer.

Therefore, considering that the efficacy of oral drug delivery particles depends on their structural fate resulting in the gut environment, future research will concern the functional *in vitro* and *in vivo* performance of the PScubosomes as an anticancer drug carrier.

## Author contributions

Barbara V. Pimenta: methodology, investigation, data curation, formal analysis. Rafael R.M. Madrid: methodology, investigation, data curation, formal analysis. Patrick D. Mathews: methodology, investigation, data curation, formal analysis. Karin A. Riske: data curation, formal analysis, writing – original draft. Watson Loh: formal analysis, validation, writing – original draft. Borislav Angelov: data curation, formal analysis, validation. Angelina Angelova: conceptualization, methodology, investigation, data curation, formal analysis, writing – original draft, writing – review & editing, supervision. Omar Mertins: conceptualization, methodology, investigation, data curation, formal analysis, supervision, writing – original draft, writing – review & editing, funding acquisition.

## Conflicts of interest

The authors declare that they have no known competing financial interests or personal relationships that could have appeared to influence the work reported in this paper.

## Acknowledgements

The authors gratefully acknowledge the allocation of beam time at Synchrotron SOLEIL (Saint Aubin, France) through the project 20191836 and the scientific and technical support of Dr T. Bizien at the SWING beamline. B. V. P. and R. R. M. M. thank CNPq for MSc and PhD fellowships. K. A. R. and O. M. thank FAPESP for the research financial support (16/13368-4 and 21/00971-2). B. A. obtained financial support from the collaborative project with JINR, Dubna (3 + 3 program, No. 204, item 27 from 25.03.2020) and the projects ''Structural Dynamics of Biomolecular Systems'' (ELI-BIO) (CZ.02.1.01/0.0/0.0/15_003/0000447) and ''Advanced research using high-intensity laser produced photons and particles'' (CZ.02. 1.01/0.0/0.0/16_019/0000789) from the European Regional Development Fund. A. A. acknowledges a membership in the CNRS GDR2088 BIOMIM research network.

## References

1 F. Wang, J. Ka, C. Lau and J. Yu, The role of natural killer cell in gastrointestinal cancer: killer or helper, *Oncogene*, 2021, **40**, 717–730, DOI: **10.1038/s41388-020-01561-z**.

2 R. K. Al-Ishaq, A. J. Overy and D. Büsselberg, Phytochemicals and gastrointestinal cancer: Cellular mechanisms and effects to change cancer progression, *Biomolecules*, 2020, **10**, 105, DOI: **10.3390/biom10010105**.

3 M. E. Schmidt, S. Scherer, J. Wiskemann and K. Steindorf, Return to work after breast cancer: The role of treatment-related side effects and potential impact on quality of life, *Eur. J. Cancer Care*, 2019, **28**, e13051, DOI: **10.1111/ecc.13051**.

4 J. Amézaga, B. Alfaro, Y. Ríos and I. Tueros, Assessing taste and smell alterations in cancer patients undergoing chemotherapy according to treatment, *Sup. Care Cancer*, 2018, **26**, 4077–4086, DOI: **10.1007/s00520-018-4277-z**.

5 N. Gianmauro, V. Longo, G. Courtho and N. Silvestris, Cancer survivorship long-term side-effects of anticancer

 

treatments of gastrointestinal cancer, *Cur. Op. Oncol.*, 2015, **27**, 351–357, DOI: 10.1097/CCO.0000000000000203.
6 J. D. Du, Q. Liu, S. Salentinig, T. H. Nguyen and B. J. Boyd, A novel approach to enhance the mucoadhesion of lipid drug nanocarriers for improved drug delivery to the buccal mucosa, *Int. J. Pharm.*, 2014, **471**, 358–365, DOI: 10.1016/j.ijpharm.2014.05.044.
7 L. Zhang, J. Li and D. Tian, *et al.*, Theranostic combinatorial drug-loaded coated cubosomes for enhanced targeting and efficacy against cancer cells, *Cell Death Dis.*, 2020, **11**, 1, DOI: 10.1038/s41419-019-2182-0.
8 N. A. D'Angelo, M. A. Noronha and M. C. C. Câmara, *et al.*, Doxorubicin nanoformulations on therapy against cancer: An overview from the last 10 years, *Biomat. Adv.*, 2022, **133**, 112623, DOI: 10.1016/j.msec.2021.112623.
9 Y. D. Dong, E. Tchung, C. Nowell, S. Kaga, N. Leong, D. Mehta, L. M. Kaminskas and B. J. Boyd, Microfluidic preparation of drug-loaded PEGylated liposomes, and the impact of liposome size on tumour retention and penetration, *J. Liposome Res.*, 2019, **29**, 1–9, DOI: 10.1080/08982104.2017.1391285.
10 G. Bor, I. D. Mat Azmi and A. Yaghmur, Nanomedicines for cancer therapy: current status, challenges and future prospects, *Therapeutic Del.*, 2019, **10**, 113–132, DOI: 10.4155/tde-2018-0062.
11 T. Li, A. J. Clulow, C. J. Nowell, A. Hawley, D. Cipolla, T. Rades and B. J. Boyd, Controlling the size and shape of liposomal ciprofloxacin nanocrystals by varying the lipid bilayer composition and drug to lipid ratio, *J. Colloid Interface Sci.*, 2019, **555**, 361–372, DOI: 10.1016/j.jcis.2019.07.081.
12 Y. Xiao, Q. Liu, A. J. Clulow, T. Li, M. Manohar, E. P. Gilbert, L. de Campo, A. Hawley and B. J. Boyd, PEGylation and surface functionalization of liposomes containing drug nanocrystals for cell-targeted delivery, *Colloids Surf., B*, 2019, **182**, 110362, DOI: 10.1016/j.colsurfb.2019.110362.
13 S. Siemer, D. Wünsch and A. Khamis, *et al.*, Nano meets micro-translational nanotechnology in medicine: Nano-based applications for early tumor detection and therapy, *Nanomaterials*, 2020, **10**, 383, DOI: 10.3390/nano10020383.
14 A. Cytryniak, K. Żelechowska-Matysiak, E. Nazaruk, R. Bilewicz, R. Walczak, E. Majka, A. Mames, F. Bruchertseifer, A. Morgenstern, A. Bilewicz and A. Majkowska-Pilip, Cubosomal lipid formulation for combination cancer treatment: Delivery of a chemotherapeutic agent and complexed a-particle emitter 213Bi, *Mol. Pharm.*, 2022, **19**, 2818–2831, DOI: 10.1021/acs.molpharmaceut.2c00182.
15 G. B. J. Glass and A. Ishimori, Passage of serum albumin into the stomach, *Am. J. Digestive Dis.*, 1961, **6**, 103–133, DOI: 10.1007/BF02231798.
16 S. Jarnum and M. Schwartz, Hypoalbuminemia in gastric carcinoma, *Gastroenterology*, 1960, **38**, 769–776, DOI: 10.1016/S0016-5085(60)80091-1.
17 S. Murgia, S. Biffi and R. Mezzenga, Recent advances of non-lamellar lyotropic liquid crystalline nanoparticles in nanomedicine, *Cur. Op. Col. Int. Sci.*, 2020, **48**, 28–39, DOI: 10.1016/j.cocis.2020.03.006.
18 A. C. Pham, T. H. Nguyen, C. J. Nowell, B. Graham and B. J. Boyd, Examining the gastrointestinal transit of lipid-based liquid crystalline systems using whole-animal imaging, *Drug Del. Trans. Res.*, 2015, **5**, 566–574, DOI: 10.1007/s13346-015-0253-z.
19 A. C. Pham, L. Hong, O. Montagnat, C. J. Nowell, T. H. Nguyen and B. J. Boyd, In vivo formation of cubic phase in situ after oral administration of cubic phase precursor formulation provides long duration gastric retention and absorption for poorly water-soluble drugs, *Mol. Pharm.*, 2016, **13**, 280–286, DOI: 10.1021/acs.molpharmaceut.5b00784.
20 Y. S. Loo, N. I. Zahid, T. Madheswaran and I. D. M. Azmi, Recent advances in the development of multifunctional lipid-based nanoparticles for co-delivery, combination treatment strategies, and theranostics in breast and lung cancer, *J. Drug Del. Sci. Tech.*, 2022, **71**, 103300, DOI: 10.1016/j.jddst.2022.103300.
21 D. G. Villalva, C. G. França and W. Loh, Characterization of cubosomes immobilized in hydrogels of hyaluronic acid and their use for diclofenac controlled delivery, *Colloids Surf., B*, 2022, **212**, 112352, DOI: 10.1016/j.colsurfb.2022.112352.
22 X. Sun, J. D. Du, A. Hawley, A. Tan and B. J. Boyd, Magnetically-stimulated transformations in the nanostructure of PEGylated phytantriol-based nanoparticles for on-demand drug release, *Colloids Surf., B*, 2021, **207**, 112005, DOI: 10.1016/j.colsurfb.2021.112005.
23 A. Angelova, M. Drechsler, V. M. Garamus and B. Angelov, Pep-lipid cubosomes and vesicles compartmentalized by micelles from self-assembly of multiple neuroprotective building blocks including a large peptide hormone PACAP-DHA, *ChemNanoMat*, 2019, **5**, 1381–1389, DOI: 10.1002/cnma.201900468.
24 Y. Li, A. Angelova, F. Hu, V. M. Garamus, C. Peng, N. Li, J. Liu, D. Liu and A. Zou, pH responsiveness of hexosomes and cubosomes for combined delivery of Brucea javanica oil and doxorubicin, *Langmuir*, 2019, **35**, 14532–14542, DOI: 10.1021/acs.langmuir.9b02257.
25 A. Angelova, V. M. Garamus, B. Angelov, Z. Tian, Y. Li and A. Zou, Advances in structural design of lipid-based nanoparticle carriers for delivery of macromolecular drugs, phytochemicals and anti-tumor agents, *Adv. Col. Interface Sci.*, 2017, **249**, 331–345, DOI: 10.1016/j.cis.2017.04.006.
26 Y. Almoshari, Development, therapeutic evaluation and theranostic applications of cubosomes on cancers: An updated review, *Pharmaceutics*, 2022, **14**, 600, DOI: 10.3390/pharmaceutics14030600.
27 R. Varghese, S. Salvi, P. Sood, B. Kulkarni and D. Kumar, *Col. Interface Sci. Com.*, 2022, **46**, 100561, DOI: 10.1016/j.colcom.2021.100561.
28 M. Mehta, V. Malyla, K. R. Paudel, D. K. Chellappan, P. M. Hansbro, B. G. Oliver and K. Dua, Berberine loaded liquid crystalline nanostructure inhibits cancer progression in adenocarcinomic human alveolar basal epithelial cells in vitro, *J. Food Biochem.*, 2021, **45**, e13954, DOI: 10.1111/jfbc.13954.

29 M. Nasr, H. Younes and R. S. Abdel-Rashid, Formulation and evaluation of cubosomes containing colchicine for transdermal delivery, *Drug Del. Trans. Res.*, 2020, **10**, 1302–1313, DOI: **10.1007/s13346-020-00785-6**.

30 A. R. Faria, O. F. Silvestre, C. Maibohm, R. M. R. Adão, B. F. B. Silva and J. B. Nieder, Cubosome nanoparticles for enhanced delivery of mitochondria anticancer drug elesclomol and therapeutic monitoring via sub-cellular NAD(P)H multi-photon fluorescence lifetime imaging, *Nano Res.*, 2018, **12**, 991–998, DOI: **10.1007/s12274-018-2231-5**.

31 E. Nazaruk, A. Majkowska-Pilip and R. Bilewicz, Lipidic cubic-phase nanoparticles-cubosomes for efficient drug delivery to cancer cells, *ChemPlusChem*, 2017, **82**, 570–575, DOI: **10.1002/cplu.201600534**.

32 P. D. Mathews, O. Mertins, B. Angelov and A. Angelova, Cubosomal lipid nanoassemblies with pH-sensitive shells created by biopolymer complexes: A synchrotron SAXS study, *J. Colloid Interface Sci.*, 2022, **607**, 440–450, DOI: **10.1016/j.jcis.2021.08.187**.

33 O. Mertins, P. D. Mathews and A. Angelova, Advances in the design of pH-sensitive cubosome liquid crystalline nanocarriers for drug delivery applications, *Nanomaterials*, 2020, **10**, 963, DOI: **10.3390/nano10050963**.

34 S. Islam, M. A. R. Bhuiyan and M. N. Islam, Chitin and chitosan: Structure, properties and applications in biomedical engineering, *J. Polym. Environ.*, 2017, **25**, 854–866, DOI: **10.1007/s10924-016-0865-5**.

35 G. Cavallaro, S. Micciulla, L. Chiappisi and G. Lazzara, Chitosan-based smart hybrid materials: a physico-chemical perspective, *J. Mater. Chem. B*, 2021, **9**, 594–611, DOI: **10.1039/D0TB01865A**.

36 P. D. Mathews and O. Mertins, Chitosan and lipid composites as versatile biomedical material, in *Materials for biomedical engineering: Nanomaterials-based drug delivery*, ed. A. M. Holban, A. M. Grumezescu, Elsevier, 2019, pp. 259–291, DOI: **10.1016/B978-0-12-816913-1.00009-X**.

37 B. B. M. Garcia, O. Mertins, E. R. Silva, P. D. Mathews and S. W. Han, Arginine-modified chitosan complexed with liposome systems for plasmid DNA delivery, *Colloids Surf., B*, 2020, **193**, 111131, DOI: **10.1016/j.colsurfb.2020.111131**.

38 R. R. M. Madrid, P. D. Mathews, A. C. M. F. Patta, A. P. Gonzales-Flores, C. A. B. Ramirez, V. L. S. Rigoni, M. Tavares-Dias and O. Mertins, Safety of oral administration of high doses of ivermectin by means of biocompatible polyelectrolytes formulation, *Heliyon*, 2021, **7**, e05820, DOI: **10.1016/j.heliyon.2020.e05820**.

39 P. D. Mathews, A. C. M. F. Patta, R. R. M. Madrid, C. A. B. Ramirez, B. V. Pimenta and O. Mertins, Efficient treatment of fish intestinal parasites applying membrane-penetrating oral drug delivery nanoparticle, *ACS Biomat. Sci. Eng.*, 2021, DOI: **10.1021/acsbiomaterials.1c00890**.

40 A. C. M. F. Patta, P. D. Mathews, R. R. M. Madrid, V. L. S. Rigoni, E. R. Silva and O. Mertins, Polyionic complexes of chitosan-N-arginine with alginate as pH responsive and mucoadhesive particles for oral drug delivery applications, *Int. J. Biol. Macromol.*, 2020, **148**, 550–564, DOI: **10.1016/j.ijbiomac.2020.01.160**.

41 R. R. M. Madrid, O. Mertins, M. Tavares-Dias, A. P. Flores-Gonzales, A. C. M. F. Patta, C. A. B. Ramirez, V. L. S. Rigoni and P. D. Mathews, High compliance and effective treatment of fish endoparasitic infections with oral drug delivery nanobioparticles: Safety of intestinal tissue and blood parameters, *J. Fish Dis.*, 2021, **44**, 1819–1829, DOI: **10.1111/jfd.13501**.

42 S. Gholamian, M. Nourani and N. Bakhshi, Formation and characterization of calcium alginate hydrogel beads filled with cumin seeds essential oil, *Food Chem.*, 2021, **338**, 128143, DOI: **10.1016/j.foodchem.2020.128143**.

43 L. Lisuzzo, G. Cavallaro, S. Milioto and G. Lazzara, Layered composite based on halloysite and natural polymers: a carrier for the pH controlled release of drugs, *New J. Chem.*, 2019, **43**, 10887–10893, DOI: **10.1039/c9nj02565k**.

44 C. A. B. Ramirez, M. M. Carriero, F. S. C. Leomil, R. L. M. Sousa, A. Miranda, O. Mertins and P. D. Mathews, Complexation of a polypeptide-polyelectrolytes bioparticle as a biomaterial of antibacterial activity, *Pharmaceutics*, 2022, **14**, 2746, DOI: **10.3390/pharmaceutics14122746**.

45 A. G. Niculescu and A. M. Grumezescu, Applications of chitosan-alginate-based nanoparticles—An up-to-date review, *Nanomaterials*, 2022, **12**, 186, DOI: **10.3390/nano12020186**.

46 K. Baler, O. A. Martin, M. A. Carignano, G. A. Ameer, J. A. Vila and I. Szleifer, Electrostatic unfolding and interactions of albumin driven by pH changes: A molecular dynamics study, *J. Phys. Chem. B*, 2014, **118**, 921–930, DOI: **10.1021/jp409936v**.

47 H. Wiig, O. Kolmannskog, O. Tenstad and J. L. Bert, Effect of charge on interstitial distribution of albumin in rat dermis in vitro, *J. Physiol.*, 2003, **550**, 505–514, DOI: **10.1113/jphysiol.2003.042713**.

48 J. F. Foster, in *Albumin structure, function and uses*. ed. V. M. Rosenoer, M. Oratz, M. A. Rothschild, Pergamon, Oxford, 1977, pp. 53–84.

49 S. Gao, A. Holkar and S. Srivastava, Protein–polyelectrolyte complexes and micellar assemblies, *Polymers*, 2019, **11**, 1097, DOI: **10.3390/polym11071097**.

50 G. David and J. Pérez, Combined sampler robot and high-performance liquid chromatography: a fully automated system for biological small-angle X-ray scattering experiments at the Synchrotron SOLEIL SWING beamline, *J. App. Crystallogr.*, 2009, **42**, 892–900, DOI: **10.1107/S0021889809029288**.

51 M. Johnsson, J. Barauskas and F. Tiberg, Cubic phases and cubic phase dispersions in a phospholipid-based system, *J. Am. Chem. Soc.*, 2005, **127**, 1076–1077, DOI: **10.1021/ja043331a**.

52 P. D. Mathews, A. C. M. F. Patta, J. V. Gonçalves, G. S. Gama, I. T. S. Garcia and O. Mertins, Targeted drug delivery and treatment of endoparasites with biocompatible particles of pH-responsive structure, *Biomacromol.*, 2018, **19**, 499–510, DOI: **10.1021/acs.biomac.7b01630**.

53 B. Jachimska and A. Pajor, Physico-chemical characterization of bovine serum albumin in solution and as deposited on surfaces, *Bioelectrochem.*, 2012, **87**, 138–146, DOI: **10.1016/j.bioelechem.2011.09.004**.


 

54 R. Curvale, M. Masuelli and A. P. Padilla, Intrinsic viscosity of bovine serum albumin conformers, *Int. J. Biol. Macromol.*, 2008, **42**, 133–137, DOI: **10.1016/j.ijbiomac.2007.10.007**.

55 R. Li, Z. Wu, Y. Wangb, L. Ding and Y. Wang, Role of pH-induced structural change in protein aggregation in foam fractionation of bovine serum albumin, *Biotech. Rep.*, 2016, **9**, 46–52, DOI: **10.1016/j.btre.2016.01.002**.

56 M. Yamasaki, H. Yano and K. Aoki, Differential scanning calorimetric studies on bovine serum albumin: I. Effects of pH and ionic strength, *Int. J. Biol. Macromol.*, 1990, **12**, 263–268, DOI: **10.1016/0141-8130(90)90007-W**.

57 C. Giancola, C. De Sena, D. Fessas, G. Graziano and G. Barone, DSC studies on bovine serum albumin denaturation effects of ionic strength and SDS concentration, *Int. J. Biol. Macromol.*, 1997, **20**, 193–204, DOI: **10.1016/S0141-8130(97)01159-8**.

58 B. Angelov, A. Angelova, V. M. Garamus, G. Lebas, S. Lesieur, M. Ollivon, S. S. Funari, R. Willumeit and P. Couvreur, Small-angle neutron and X-ray scattering from amphiphilic stimuli-responsive diamond type bicontinuous cubic phase, *J. Am. Chem. Soc.*, 2007, **129**, 13474–13479, DOI: **10.1021/ja072725**.

59 P. D. Mathews and O. Mertins, Dispersion of chitosan in liquid crystalline lamellar phase: Production of biofriendly hydrogel of nano cubic topology, *Carbohydr. Polym.*, 2017, **157**, 850–857, DOI: **10.1016/j.carbpol.2016.10.071**.

60 H. Zhou and D. J. McClements, Recent advances in the gastrointestinal fate of organic and inorganic nanoparticles in foods, *Nanomaterials*, 2022, **12**, 1099, DOI: **10.3390/nano12071099**.

61 M. Hu, Y. Li, E. A. Decker, H. Xiao and D. J. McClements, Influence of tripolyphosphate cross-linking on the physical stability and lipase digestibility of chitosan-coated lipid droplets, *J. Agric. Food Chem.*, 2010, **58**, 1283–1289, DOI: **10.1021/jf903270y**.